



# Radiomics and deep learning for large volume lymph node metastasis in papillary thyroid carcinoma

Zhongkai Ni<sup>1#</sup>, Tianhan Zhou<sup>1#</sup>, Hao Fang<sup>2#</sup>, Xiangfeng Lin<sup>3#</sup>, Zhiyu Xing<sup>4</sup>, Xiaowen Li<sup>1</sup>, Yangyang Xie<sup>5</sup>, Lihua Hong<sup>1</sup>, Shifei Huang<sup>1</sup>, Jinwang Ding<sup>6</sup>, Hai Huang<sup>1</sup>

<sup>1</sup>Department of General Surgery, Hangzhou Hospital of Traditional Chinese Medicine, Hangzhou, China; <sup>2</sup>Hangzhou Clinical Medical College, Zhejiang Chinese Medicine University, Hangzhou, China; <sup>3</sup>Department of Thyroid Surgery, Affiliated Yantai Yuhuangding Hospital, Qingdao University, Yantai, China; <sup>4</sup>Department of Ultrasonography, Affiliated Hangzhou First People's Hospital, Westlake University, School of Medicine, Hangzhou, China; <sup>5</sup>Key Laboratory of Laparoscopic Technology of Zhejiang Province, Department of General Surgery, Sir Run-Run Shaw Hospital, Zhejiang University School of Medicine, Hangzhou, China; <sup>6</sup>Department of Head and Neck Surgery, Cancer Hospital of the University of Chinese Academy of Sciences, Hangzhou, China

**Contributions:** (I) Conception and design: Z Ni, T Zhou, H Huang, J Ding; (II) Administrative support: Z Xing; H Fang; (III) Provision of study materials or patients: X Lin; (IV) Collection and assembly of data: S Huang; (V) Data analysis and interpretation: X Li, Y Xie; (VI) Manuscript writing: All authors; (VII) Final approval of manuscript: All authors.

<sup>#</sup>These authors contributed equally to this work.

**Correspondence to:** Hai Huang, PhD. Department of General Surgery, Hangzhou Hospital of Traditional Chinese Medicine, 453 Stadium Road, Hangzhou 310007, China. Email: tcmhuanghai@163.com; Jinwang Ding, MD. Department of Head and Neck Surgery, Cancer Hospital of the University of Chinese Academy of Sciences, 38 Guangji Road, Hangzhou 310005, China. Email: zjlsdjw@163.com.

**Background:** Thyroid cancer is prone to early lymph node metastasis (LNM), and patients with large volume LNM (LVLNM) tend to have a poorer prognosis. The aim of this study was to predict LVLNM in before surgery based on radiomics and deep learning (DL).

**Methods:** A multicenter retrospective study was performed, including 854 papillary thyroid carcinoma (PTC) patients from three centers. Radiomics features were extracted. Logistic regression (LR), support vector machine (SVM), K-nearest neighbors (KNN), multi-layer perceptron (MLP), random forest (RF), ExtraTrees, extreme gradient boosting (XGBoost), and light gradient boosting machine (LightGBM) algorithms were used to construct radiomics models. AlexNet, DenseNet121, inception\_v3, ResNet50, and transformer algorithms were used to construct DL models. The receiver operating characteristic (ROC) curve was employed to select the better-performing model. A combined model was then created by merging radiomics features and DL features. The least absolute shrinkage and selection operator (LASSO) method was utilized to identify metabolites and radiomics features with non-zero coefficients. The performance of the models was evaluated using area under the curve (AUC), accuracy (ACC), sensitivity (SEN), specificity (SPE), positive predictive value (PPV), negative predictive value (NPV), and F1-score.

**Results:** A total of 1,357 radiomics features were extracted. Among the radiomics models, the ExtraTrees model demonstrated the optimal diagnostic capabilities with an AUC of 0.787 [95% confidence interval (CI): 0.715–0.858], and DenseNet121 DL model demonstrated the optimal diagnostic capabilities with an AUC of 0.766 (95% CI: 0.683–0.848). Furthermore, the combined model, named the Thy-DL-Radiomics model, exhibited an AUC of 0.839 (95% CI: 0.758–0.920) in the internal validation set and 0.789 (95% CI: 0.718–0.859) in the external validation set.

**Conclusions:** A radiomics-DL features integrated model can predict LVLNM in PTC patients and provide guidance for personalized treatment.

**Keywords:** Radiomics; deep learning (DL); machine learning (ML); large volume lymph node metastasis (LVLNM); papillary thyroid carcinoma (PTC)

Submitted Jul 19, 2024. Accepted for publication Aug 28, 2024. Published online Sep 18, 2024.

doi: 10.21037/gs-24-308

View this article at: <https://dx.doi.org/10.21037/gs-24-308>

## Introduction

Thyroid cancer is the fastest-growing endocrine malignancy globally, with papillary thyroid carcinoma (PTC) accounting for over 90% of cases (1). Upon diagnosis, 25–80% of PTC patients already exhibit lymph node metastasis (LNM) in the neck, even when tumor diameters are  $\leq 1$  cm, with a metastatic rate of 12–64% (2–4). Although PTC generally has a favorable prognosis, with a 10-year survival rate exceeding 88%, cervical LNM significantly increases the risk of recurrence and mortality (5). Specifically, if more than five lymph nodes are involved, the postoperative recurrence rate exceeds 30% (6). The American Thyroid Association (ATA) guidelines stratify the risk of recurrence and suggest that PTC patients with more than five metastatic lymph nodes are at moderate or high recurrence risk, indicating a preoperative inclination towards proactive preventative lymph node dissection (7). Previous research has reported that when the number of metastatic lymph

nodes exceeds five, it is typically defined as large volume LNM (LVLNM) (8). Currently, lymph node dissection is indisputably required for patients with moderate- or high-risk of recurrence, but the necessity of prophylactic dissection for patients with a low-risk of recurrence remains controversial. Recent opinions suggest that active surveillance (AS) could replace surgical treatment for low-risk PTC to avoid unnecessary harm from overtreatment (9). Therefore, accurate preoperative assessment of LNM is crucial.

Ultrasound is commonly used preoperatively to assess the presence of LNM in PTC (10). However, due to the deep location and obstruction by the surrounding tissue in the central neck region, the sensitivity (SEN) of ultrasound to detect central LNM is low, ranging from only 31% to 35% (11). Computed tomography (CT), with its higher spatial resolution, can clearly display suspicious metastatic lymph nodes and their relationship with surrounding structures, with a SEN of 47–63% and specificity (SPE) of 90–95% (12). However, the evaluation of cervical LNM by radiologists is time-consuming and subjective, often depending on the radiologist's experience and imaging equipment. In recent years, radiomics has garnered significant attention in precise diagnosis. Li *et al.* proposed a radiomics-based approach predicting LNM in PTC patients by converting ultrasound image features such as intensity, boundary, texture, and wavelet into extractable data (13). Concurrently, deep learning (DL), a new scientific technology, has been used in medical imaging research to overcome limitations in manual image analysis and information retrieval.

This study aims to develop a combined DL-Radiomics model to enhance the preoperative prediction of LVLNM in patients with PTC, striving to provide more precise individualized diagnostic and therapeutic plans. By integrating the strengths of radiomics and DL, we expect this model to improve the accuracy (ACC) of LNM quantification, thus aiding in better risk stratification and treatment decisions for PTC patients. We present this article in accordance with the TRIPOD reporting checklist (available at <https://gs.amegroups.com/article/view/10.21037/gs-24-308/rc>).

### Highlight box

#### Key findings

- The Thy-deep learning (DL)-Radiomics model was developed to predict large volume lymph node metastasis (LVLNM) in patients with papillary thyroid carcinoma (PTC), demonstrating an area under the curve of 0.839 in internal validation and 0.789 in external validation. By integrating radiomics and DL features, this model provides personalized diagnostic and therapeutic insights for PTC patients.

#### What is known and what is new?

- Current knowledge encompasses the use of ultrasound imaging and clinical features to predict lymph node metastasis (LNM), though the accuracy (ACC) of these methods requires enhancement.
- The innovative Thy-DL-Radiomics model signifies a significant advancement by integrating radiomics and DL techniques to improve the risk assessment of LNM in patients with PTC.

#### What is the implication, and what should change now?

- The implications of the Thy-DL-Radiomics model include the enhanced identification of high-risk LVLNM patients, which could potentially inform personalized treatment strategies and improve patient outcomes. It is recommended that clinicians incorporate advanced imaging and machine learning models into clinical practice to enhance the ACC of preoperative assessments in PTC.

## Methods

### *Patients*

This study collected data from patients with PTC who underwent surgery at Hangzhou Hospital of Traditional Chinese Medicine, Cancer Hospital of the University of Chinese Academy of Sciences, Affiliated Yantai Yuhuangding Hospital, Qingdao University from January 2023 to December 2023. The data were divided into a training set, an internal validation set, and an external validation set. The inclusion criteria were as follows: (I) pathological confirmation of PTC; (II) patients who underwent primary surgery accompanied by cervical lymph node dissection; (III) postoperative pathological reports including detailed information on the number of lymph nodes dissected and the number of metastatic lymph nodes; and (IV) availability of comprehensive preoperative thyroid ultrasound images for analysis. The exclusion criteria were as follows: (I) postoperative pathological diagnosis indicating sub-types of PTC; (II) history of neck trauma, previous tumor surgery, or adjuvant chemoradiotherapy; and (III) fewer than three lymph nodes dissected during surgery. The surgical procedures were listed in [Appendix 1](#). The study was conducted in accordance with the Declaration of Helsinki (as revised in 2013). The study was approved by the Ethics Committee of Hangzhou Hospital of Traditional Chinese Medicine (No. 2022KY153-CX1). All participating hospitals were informed and agreed with this study. Individual consent for this retrospective analysis was waived.

### *Imaging acquisition and thyroid nodules segmentation*

A color Doppler ultrasound machine equipped with a real-time, high-frequency (5–12 MHz) linear-array probe was used in this study. The ultrasound image data was collected by two ultrasound radiologists with 5 years of thyroid ultrasound experience. The images of the thyroid nodules were stored in JPG format. The regions of interest (ROIs) of the PTCs were manually delineated using ITK-SNAP (version 3.6.0). A radiologist with 10 years of experience outlined the ROI borders for the thyroid nodules.

### *Radiomics feature extraction and selection*

The data extracted included first-order features, intensity histogram statistics, shape and size statistics, and (filtered) texture features. All handcrafted features were extracted using an in-house feature analysis program implemented

in Pyradiomics (<http://pyradiomics.readthedocs.io>). The explanation was listed in [Appendix 2](#). The least absolute shrinkage and selection operator (LASSO) regression model was applied to the training dataset for signature construction. LASSO shrinks all regression coefficients towards zero and sets the coefficients of many irrelevant features to zero depending on the regulation weight  $\lambda$ . To find the optimal  $\lambda$ , a 5-fold cross-validation with minimum criteria was employed, wherein the final value of  $\lambda$  yielded the minimum cross-validation error. The retained features with nonzero coefficients were used for fitting the regression model and were combined into a radiomics feature.

### *The construction of a DL model and DL feature extraction*

In thyroid ultrasound images, each image has a corresponding mask image containing the cancerous region, where the pixels of the cancerous area are set to 255, and other non-cancerous areas are set to 0. We extracted the ROI of the nodule area based on the image mask, defining the minimum bounding rectangle. We utilized two-dimensional (2D) ultrasound grayscale images as input. The model output was the probability of LVLNM in PTC. The training parameters are presented in [Appendix 3](#). To enhance the network's generalization ability, random data transformations were applied during training batches based on different task characteristics. This allowed the network to learn geometric invariance, such as size changes, rotations, affine transformations, contrast variations, noise interference, to reduce variations arising from the diverse physical properties of different ultrasound devices. We derived a set of DL features from the previously described pre-trained DL model. Initially, each image in the dataset underwent processing through the model, and the output activations of the second-to-last fully-connected neural network (FCNN) layer were retained and utilized as the DL features of the images. Principal component analysis (PCA) was conducted to further reduce the dimensionality of DL features to 128. We utilized the Gradient-weighted Class Activation Map (Grad-CAM) algorithm to visualize heatmaps that highlight the image regions contributing most to the model prediction. Specifically, we applied Grad-CAM to the final convolutional layer in our model to generate heatmaps with appropriate spatial resolution (14).

### *Combined radiomics and DL features*

To construct the integrated DL-Radiomics model, DL

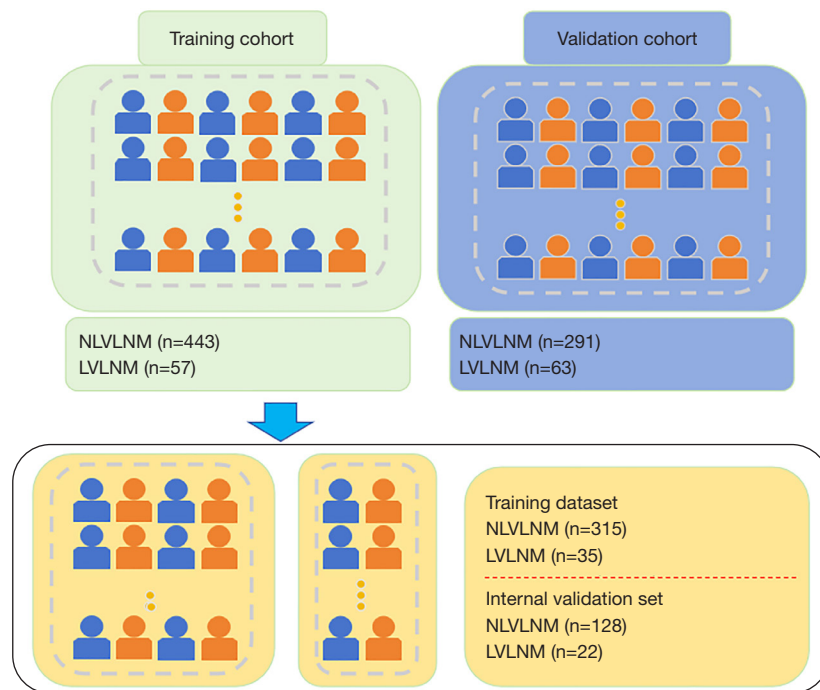


**Figure 1** Flow chart of patient recruitment. NLVLNM, non-large volume lymph node metastasis; LVLNM, large volume lymph node metastasis.

features were merged with the radiomics features to create a combined set of DL-radiomics features for each image. For classifier selection, the development dataset was split into training dataset and internal validation dataset portions for the examination and evaluation of seven different classifiers: logistic regression (LR), support vector machine (SVM), K-nearest neighbors (KNN), multi-layer perceptron (MLP), random forest (RF), ExtraTrees, extreme gradient boosting (XGBoost), and light gradient boosting machine (LightGBM). The machine learning (ML) classifier demonstrated the highest area under the curve (AUC) in the highest average and lowest standard deviation (SD) across 5-fold cross-validations, leading to its adoption for the optimal model development.

### Statistical analysis

By employing descriptive statistics, mean values and SDs characterized the ages and sizes of the nodules. The classification outcomes from each method were detailed through both absolute quantities and percentages relative to the gold standard. The statistical evaluation each model regarding the gold standard included metrics such as

AUC, ACC, SEN, SPE, positive predictive value (PPV), negative predictive value (NPV), and F1-score to assess result consistency. Statistical tests for the  $\kappa$  coefficient across different groups were performed, and group comparisons utilized the  $\chi^2$  test, alongside the analysis of receiver operating characteristic (ROC) curves. DeLong tests were conducted to compare the AUCs. For statistical significance, a P value  $<0.05$  was considered. R software version 4.0.2 (R Foundation for Statistical Computing, Vienna, Austria) was utilized for all statistical analyses. The statistical analyses were executed using R software (version 4.3.1).

## Results

### Patient cohort

This study enrolled 854 patients diagnosed with PTC, comprising 212 males and 642 females, with an age distribution of  $45.89 \pm 12.19$  years, ranging from 18 to 85 years. Of the 854 PTC patients, there were 414 patients without LNM, 340 patients with LNM but less than 5, and 120 patients with LVLNM. These patients were segregated into three cohorts: a training set ( $n=350$ ), internal validation set ( $n=150$ ), and external validation set ( $n=374$ ). *Figures 1,2*

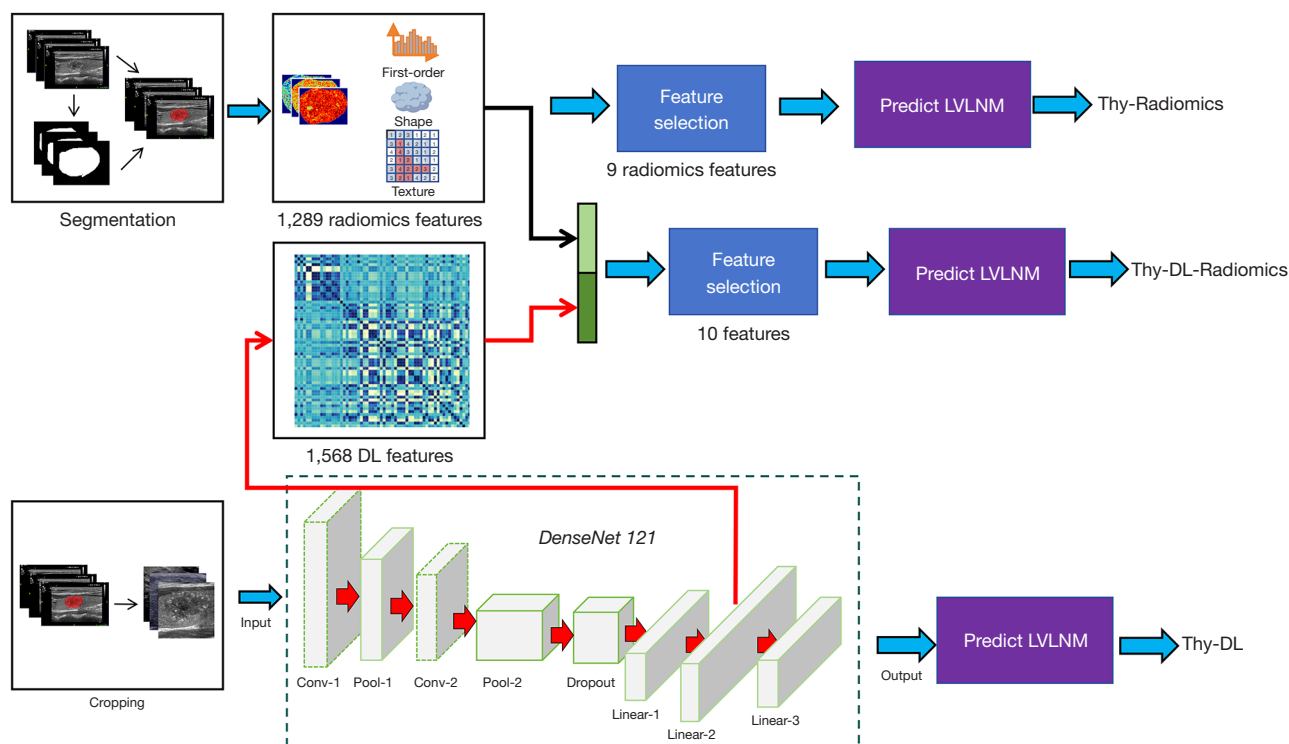


**Figure 2** Development of three LVLNM prediction models: Thy-Radiomics, Thy-DL, and combined Thy-DL-Radiomics. LVLNM, large volume lymph node metastasis; DL, deep learning.

illustrate the study's flow diagram. Clinical data are detailed in *Table 1*.

### ***Radiomics features selection and radiomics model building***

A total of seven categories and 1,357 radiomics features were extracted, including 374 first-order, 14 shape, and 969 texture features. We included 1–3 representative ultrasound images for each patient without limitation of transverse and longitudinal cuts, and satisfactory reproducibility of radiomics feature extraction was achieved. LASSO was employed in the training cohort to determine the optimal regulation weight, and 9 RFs were chosen for predicting LVLNM (*Figure 3A*). The Thy-Radiomics model was obtained by ExtraTrees algorithm compared with eight classical ML model classifiers (*Table 2*). *Figure 3B* shows the AUC of each ML model on the internal validation set cohort of the Thy-Radiomics model. The Thy-Radiomics model achieved the best value of AUC reaching 0.787 [95% confidence interval (CI): 0.715–0.858] for predicting the

LVLNM by ExtraTrees. The ACC, SEN, SPE, PPV, NPV, and F1-score of the ExtraTrees model were 0.718, 0.738, 0.714, 0.33, 0.935, and 0.456 respectively (*Figure 3C*). Then, we conducted a five random cross-validation of the internal dataset (*Table S1*).

### ***DL model building and DL features selection***

We further tried five DL models to assess the risk of LVLNM in PTC, including AlexNet, DenseNet121, inception\_v3, ResNet50, and transformer algorithm to select the optimal DL model. *Table 2* shows the AUC of performance of DL model. The Thy-DL model by DenseNet121 showed the best result with an AUC of 0.766 (95% CI: 0.683–0.848). The ACC, SEN, SPE, PPV, NPV, and F1-score of the DenseNet121 model were 0.721, 0.714, 0.723, 0.33, 0.714, and 0.451, respectively, in predicting LVLNM (*Table 2*). We further extracted the DenseNet121 model of DL features, in which 1,568 DL features were extracted. The dimensionality of DL features was reduced to 128 features by PCA.



**Table 1** The baseline characteristics of the PTC patients

Characteristics	Training set (n=350)		Internal validation set (n=150)		External verification set (n=374)	
	NLVLNM	LVLNM	NLVLNM	LVLNM	NLVLNM	LVLNM
Sex						
Female	246	21	96	16	222	41
Male	69	14	32	6	69	22
Age (years)	42.11±15.34	47.32±9.27	41.61±14.54	39.45±9.35	46.31±12.51	42.11±13.21
Size (mm)	7.36±3.26	12.63±5.38	9.38±4.25	12.35±3.51	8.96±5.13	13.43±4.67
Multifocality						
No	200	17	50	15	227	45
Yes	115	18	78	7	64	18
Capsular invasion						
No	263	5	84	4	141	9
Yes	52	30	44	18	150	54

Data are presented as number or mean ± SD. PTC, papillary thyroid carcinoma; NLVLNM, non-large volume lymph node metastasis; LVLNM, large volume lymph node metastasis; SD, standard deviation.

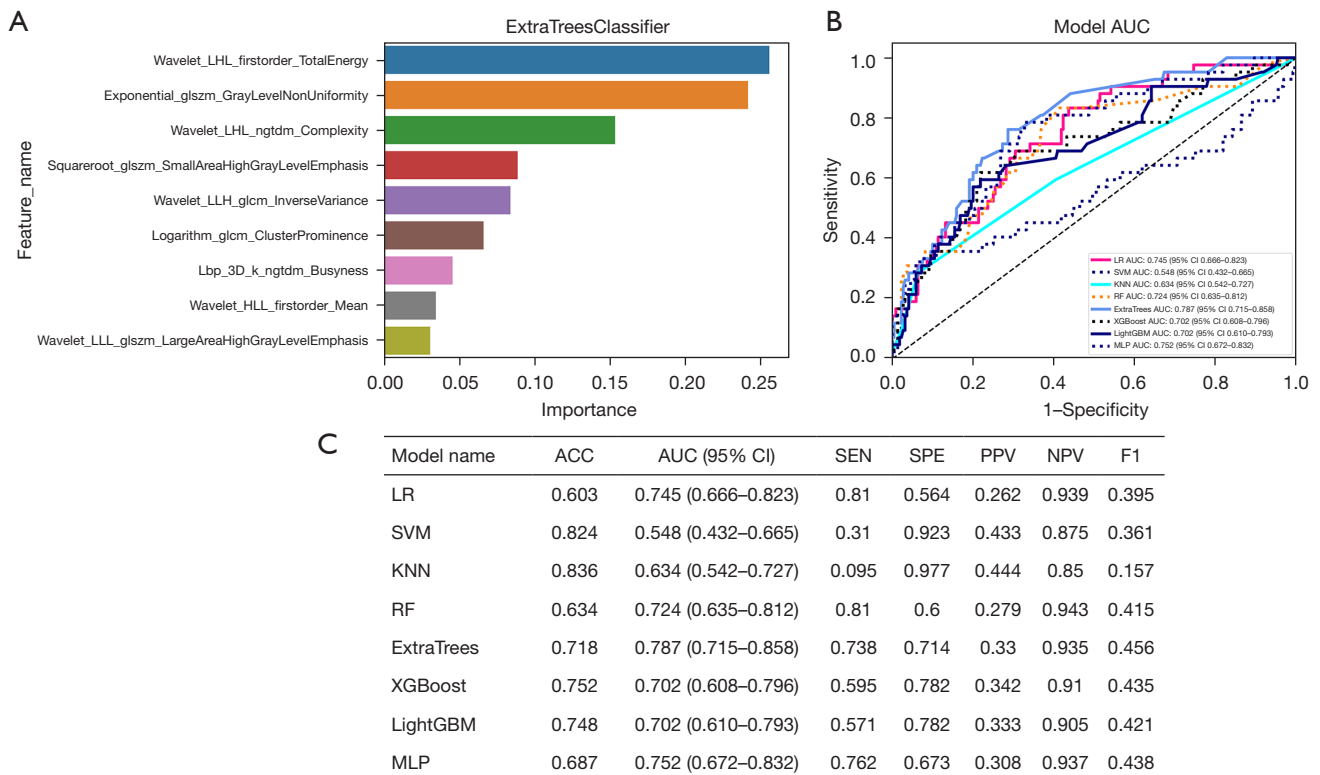


**Figure 3** The performance of Thy-Radiomics models. (A) The nine radiomics features were selected to build radiomics models. (B) The ROC of different ML models. (C) The performance of different ML models. 3D, three-dimensional; AUC, area under the curve; LR, logistic regression; CI, confidence interval; SVM, support vector machine; KNN, K-nearest neighbors; RF, random forest; XGBoost, extreme gradient boost; LightGBM, light gradient boosting machine; MLP, multi-layer perceptron; ACC, accuracy; SEN, sensitivity; SPE, specificity; PPV, positive predictive value; NPV, negative predictive value; F1, F1-score; ROC, receiver operating characteristic; ML, machine learning.

**Table 2** The results of DL models

Model name	ACC	AUC (95% CI)	SEN	SPE	PPV	NPV	F1
AlexNet	0.641	0.735 (0.652–0.818)	0.738	0.623	0.272	0.738	0.397
DenseNet121	0.721	0.766 (0.683–0.848)	0.714	0.723	0.33	0.714	0.451
Inception_v3	0.34	0.492 (0.411–0.572)	0.857	0.241	0.177	0.857	0.294
ResNet50	0.676	0.686 (0.600–0.772)	0.619	0.686	0.274	0.619	0.38
ViT	0.794	0.614 (0.528–0.700)	0.19	0.909	0.286	0.19	0.229

DL, deep learning; ACC, accuracy; AUC, area under the curve; CI, confidence interval; SEN, sensitivity; SPE, specificity; PPV, positive predictive value; NPV, negative predictive value; F1, F1-score; ViT, vision transformer.

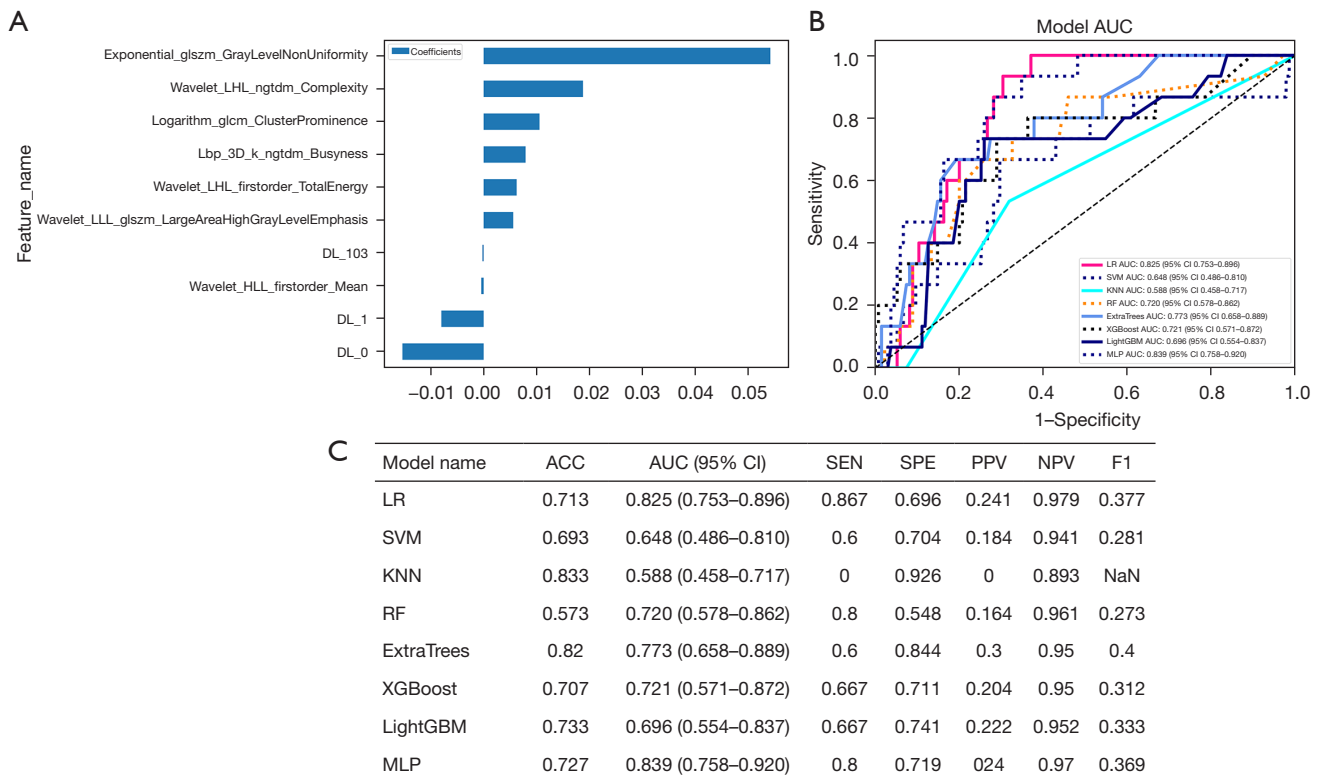
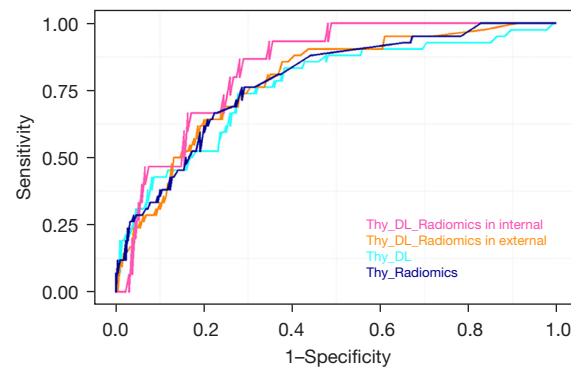


**Figure 4** The performance of Thy-DL-Radiomics. (A) The seven radiomics features and three DL features were selected to build radiomics models. (B) The ROC of different RFs and DL features combined models. (C) The performance of different combined models in the internal validation set. 3D, three-dimensional; DL, deep learning; AUC, area under the curve; LR, logistic regression; CI, confidence interval; SVM, support vector machine; KNN, K-nearest neighbors; RF, random forest; XGBoost, extreme gradient boost; LightGBM, light gradient boosting machine; MLP, multi-layer perceptron; ACC, accuracy; SEN, sensitivity; SPE, specificity; PPV, positive predictive value; NPV, negative predictive value; F1, F1-score; ROC, receiver operating characteristic.

**Combined model and performance evaluation**

We further integrated the aforementioned RFs and DL features. After a screening process, we selected seven traditional radiomics features and three DL features to

predict LVLNM (Figure 4). We constructed a combined model, named the Thy-DL-Radiomics model, for which the internal validation set results showed an AUC of 0.839 (95% CI: 0.758–0.920), and the ACC, SEN, SPE, PPV,



Model name	ACC	AUC (95% CI)	SEN	SPE	PPV	NPV	F1
Thy-DL-Radiomics in internal data	0.727	0.839 (0.758–0.920)	0.8	0.719	0.24	0.97	0.369
Thy-DL-Radiomics in external data	0.658	0.789 (0.718–0.859)	0.833	0.624	0.297	0.952	0.437
Thy-DL	0.721	0.766 (0.683–0.848)	0.714	0.723	0.33	0.714	0.451
Thy-Radiomics	0.718	0.787 (0.715–0.858)	0.738	0.714	0.33	0.935	0.456

**Figure 5** The compared models in Thy-DL-Radiomics in internal data, Thy-DL-Radiomics in external data, Thy-DL, and Thy-Radiomics. DL, deep learning; ACC, accuracy; AUC, area under the curve; CI, confidence interval; SEN, sensitivity; SPE, specificity; PPV, positive predictive value; NPV, negative predictive value; F1, F1-score.

NPV, and F1-score of MLP were 0.727, 0.8, 0.719, 0.24, 0.97, and 0.369, respectively. To assess the performance of the Thy-DL-Radiomics model on an external test set, we included PTC patients as an external validation set, which yielded an AUC of 0.789 (95% CI: 0.718–0.859). The ACC, SEN, SPE, PPV, NPV, and F1-score of the Thy-DL-Radiomics model were 0.658, 0.833, 0.624, 0.297, 0.952, and 0.437, respectively, in predicting LVLNM. Additionally, the DeLong test results indicated that the Thy-DL-Radiomics model in the internal validation set showed better performance in predicting LVLNM ( $P < 0.05$ , Figure 5).

### Model interpretability

We extracted visual inspection information of images processed in the final convolutional layer of the DL algorithm, showcasing the capability to handle ultrasound imaging data in diverse ways. Simultaneously, we characterized the distinct features of diverse imaging radiomics, as shown in Figure 6.

### Discussion

This study developed a new preoperative method for

assessing LVLNM based on PTC ultrasound. By analyzing ultrasound radiomics features and DL algorithms, we successfully constructed a model combining radiomics features and DL features to predict LVLNM. Our results demonstrate the feasibility of predicting LNM in PTC through the fusion of convolutional neural network (CNN) algorithms and radiomics features.

The literature reports that qualitative ultrasound features extracted from PTC primary lesions in ultrasound images (such as tumor size, location, and echogenicity) achieved an ACC of 71.2% (15). Wu *et al.* used ultrasound images to evaluate LNM in PTC patients, and concluded that tumor size, blood flow, and Hashimoto's thyroiditis were independent factors for LNM (16). Nie *et al.* found that tumor size, tumor invasiveness, and tumor location were significantly associated with LNM in the univariate analysis (17). This confirmed the value of using ultrasound image features of primary lesions to predict LNM. In this study, radiomics features, imperceptible to the naked eye, were extracted, revealing clinical information that might evade detection by clinicians. Various ML algorithms were further employed to reduce feature complexity and select the optimal feature combinations (18). Unlike traditional methods, DL as a data-driven end-to-end



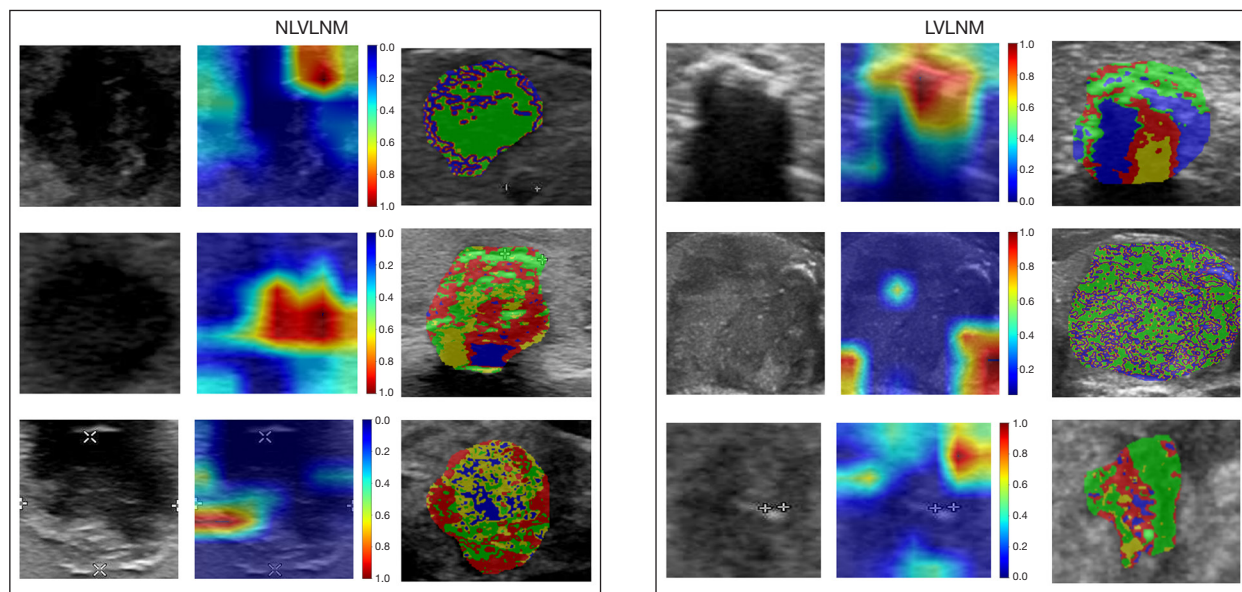


**Figure 6** Heatmaps for PTC by Grad-CAM displaying the importance of different image regions to the network decision of identifying LVLNM and heatmaps for PTC by sub-region analysis displaying the importance of radiomics different sub-region. NLVLNM, non-large volume lymph node metastasis; LVLNM, large volume lymph node metastasis; PTC, papillary thyroid cancer; Grad-CAM, Gradient-weighted Class Activation Map.

learning approach typically does not require preprocessing. Its training process inherently involves feature extraction and optimal selection, eliminating the need for classifier selection. With the advancement of hardware-like graphic processors, DL excels in handling big data, enabling rapid processing and computation. Additionally, DL can automatically extract high-dimensional, high-level features, superior to traditionally designed features, and does not require subsequent selection (19). This study utilized 1,568 DL features to evaluate the risk of LVLNM metastasis, offering a more accurate and objective approach to image feature extraction as compared to human observation, reducing inter-observer variability and saving substantial manpower.

The Thyroid Imaging Reporting and Data System (TI-RADS) scoring system based on different ultrasound characteristics such as calcification, echo patterns, and margins, was developed to assess the malignancy of thyroid nodules (20). However, radiomics features, as high-dimensional features, lack interpretability (21). This study identified nine radiomics features closely associated with LVLNM using ML algorithms. Therefore, we introduced a new habitat analysis technique. By characterizing the differential features between the LVLNM group and the

non-LVLNM (NLVLNM) group, the optimal category was identified through cluster analysis (22). Visual analysis of the results indicated that calcification in hypoechoic regions was correlated with LVLNM, consistent with previous research (23). DL, being a black-box model, also faces challenges with interpretability. Grad-CAM weights and integrates gradients of the neural network's output to visualize the model's focus on specific regions and crucial predictive information, aiding in the understanding and interpretation of the model's operational principles (24). Jia *et al.* found that the GAFM-Hybrid model may help identify novel diagnosis-relevant second-order features beyond ultrasonography to assess the malignancy of thyroid nodules (25). Further selection of DL features related to LVLNM using DL algorithms requires future research.

This study also has certain limitations. Firstly, to meet the demands of large sample sizes required for DL, it is necessary to further incorporate samples from multiple centers to increase the sample size, assess the model's external generalization ability, and further enhance the model's robustness. This study included 1–3 ultrasound images from different planes to evaluate LVLNM. In future research, it is essential to investigate the impact of the quantity of ultrasound images and planes on the results.

The LNM of PTC is complex; this study was limited to the presence of LVLNM in lymph nodes. Further exploration is needed regarding the location, region, and quantity of LNM to meet precise clinical requirements.

## Conclusions

A combined Thy-DL-Radiomics model utilizing thyroid ultrasound images surpasses the performance of standalone DL or radiomics models in predicting LVLNM in PTC patients, serving as an effective screening tool potentially informing decisions about surgery administration. These AI models hold promise for providing noninvasive and convenient preoperative guidance. However, despite their potential, the clinical utility of such screening models is currently limited, necessitating further research to enhance their ACC and generalizability.

## Acknowledgments

Some of our experiments were carried out on the OnekeyAI platform. We thank OnekeyAI and their developers' help in this scientific research work.

*Funding:* This study was funded by the Zhejiang Traditional Medicine and Technology Program, China (No. 2022ZA119).

## Footnote

*Reporting Checklist:* The authors have completed the TRIPOD reporting checklist. Available at <https://gs.amegroups.com/article/view/10.21037/gc-24-308/rc>

*Data Sharing Statement:* Available at <https://gs.amegroups.com/article/view/10.21037/gc-24-308/dss>

*Peer Review File:* Available at <https://gs.amegroups.com/article/view/10.21037/gc-24-308/prf>

*Conflicts of Interest:* All authors have completed the ICMJE uniform disclosure form (available at <https://gs.amegroups.com/article/view/10.21037/gc-24-308/coif>). The authors have no conflicts of interest to declare.

*Ethical Statement:* The authors are accountable for all aspects of the work in ensuring that questions related to the accuracy or integrity of any part of the work are appropriately investigated and resolved. The study was conducted in accordance with the Declaration of Helsinki

(as revised in 2013). The study was approved by the Ethics Committee of Hangzhou Hospital of Traditional Chinese Medicine (No. 2022KY153-CX1). All participating hospitals were informed and agreed with this study. Individual consent for this retrospective analysis was waived.

*Open Access Statement:* This is an Open Access article distributed in accordance with the Creative Commons Attribution-NonCommercial-NoDerivs 4.0 International License (CC BY-NC-ND 4.0), which permits the non-commercial replication and distribution of the article with the strict proviso that no changes or edits are made and the original work is properly cited (including links to both the formal publication through the relevant DOI and the license). See: <https://creativecommons.org/licenses/by-nc-nd/4.0/>.

## References

1. Siegel RL, Miller KD, Wagle NS, et al. Cancer statistics, 2023. *CA Cancer J Clin* 2023;73:17-48.
2. Xu S, Huang H, Huang Y, et al. Comparison of Lobectomy vs Total Thyroidectomy for Intermediate-Risk Papillary Thyroid Carcinoma With Lymph Node Metastasis. *JAMA Surg* 2023;158:73-9.
3. van Dijk SPJ, Coerts HI, Gunput STG, et al. Assessment of Radiofrequency Ablation for Papillary Microcarcinoma of the Thyroid: A Systematic Review and Meta-analysis. *JAMA Otolaryngol Head Neck Surg* 2022;148:317-25.
4. Chen DW, Lang BHH, McLeod DSA, et al. Thyroid cancer. *Lancet* 2023;401:1531-44.
5. Xiao L, Zhou J, Tan W, et al. Contrast-enhanced US with Perfluorobutane to Diagnose Small Lateral Cervical Lymph Node Metastases of Papillary Thyroid Carcinoma. *Radiology* 2023;307:e221465.
6. Machens A, Dralle H. Correlation between the number of lymph node metastases and lung metastasis in papillary thyroid cancer. *J Clin Endocrinol Metab* 2012;97:4375-82.
7. Haugen BR, Alexander EK, Bible KC, et al. 2015 American Thyroid Association Management Guidelines for Adult Patients with Thyroid Nodules and Differentiated Thyroid Cancer: The American Thyroid Association Guidelines Task Force on Thyroid Nodules and Differentiated Thyroid Cancer. *Thyroid* 2016;26:1-133.
8. Oh HS, Park S, Kim M, et al. Young Age and Male Sex Are Predictors of Large-Volume Central Neck Lymph Node Metastasis in Clinical N0 Papillary Thyroid Microcarcinomas. *Thyroid* 2017;27:1285-90.
9. Cho SJ, Suh CH, Baek JH, et al. Active Surveillance for

- Small Papillary Thyroid Cancer: A Systematic Review and Meta-Analysis. *Thyroid* 2019;29:1399-408.
10. Kambalapalli M, Gupta A, Prasad UR, et al. Ultrasound characteristics of the thyroid in children and adolescents with goiter: a single center experience. *Thyroid* 2015;25:176-82.
  11. Lee DW, Ji YB, Sung ES, et al. Roles of ultrasonography and computed tomography in the surgical management of cervical lymph node metastases in papillary thyroid carcinoma. *Eur J Surg Oncol* 2013;39:191-6.
  12. Wang C, Yu P, Zhang H, et al. Artificial intelligence-based prediction of cervical lymph node metastasis in papillary thyroid cancer with CT. *Eur Radiol* 2023;33:6828-40.
  13. Li F, Pan D, He Y, et al. Using ultrasound features and radiomics analysis to predict lymph node metastasis in patients with thyroid cancer. *BMC Surg* 2020;20:315.
  14. Iqbal S, Qureshi AN, Alhussein M, et al. AD-CAM: Enhancing Interpretability of Convolutional Neural Networks with a Lightweight Framework - From Black Box to Glass Box. *IEEE J Biomed Health Inform* 2023. [Epub ahead of print]. doi: 10.1109/JBHI.2023.3329231.
  15. Liu T, Zhou S, Yu J, et al. Prediction of Lymph Node Metastasis in Patients With Papillary Thyroid Carcinoma: A Radiomics Method Based on Preoperative Ultrasound Images. *Technol Cancer Res Treat* 2019;18:1533033819831713.
  16. Wu Q, Li Y, Wang Y, et al. Sonographic features of primary tumor as independent predictive factors for lymph node metastasis in papillary thyroid carcinoma. *Clin Transl Oncol* 2015;17:830-4.
  17. Nie X, Tan Z, Ge M, et al. Risk factors analyses for lateral lymph node metastases in papillary thyroid carcinomas: a retrospective study of 356 patients. *Arch Endocrinol Metab* 2016;60:492-9.
  18. Yu B, Li Y, Yu X, et al. Differentiate Thyroid Follicular Adenoma from Carcinoma with Combined Ultrasound Radiomics Features and Clinical Ultrasound Features. *J Digit Imaging* 2022;35:1362-72.
  19. Peng S, Liu Y, Lv W, et al. Deep learning-based artificial intelligence model to assist thyroid nodule diagnosis and management: a multicentre diagnostic study. *Lancet Digit Health* 2021;3:e250-9.
  20. Tessler FN, Middleton WD, Grant EG. Thyroid Imaging Reporting and Data System (TI-RADS): A User's Guide. *Radiology* 2018;287:29-36.
  21. Jiang L, Guo S, Zhao Y, et al. Predicting Extrathyroidal Extension in Papillary Thyroid Carcinoma Using a Clinical-Radiomics Nomogram Based on B-Mode and Contrast-Enhanced Ultrasound. *Diagnostics (Basel)* 2023;13:1734.
  22. Wu J, Gensheimer MF, Zhang N, et al. Tumor Subregion Evolution-Based Imaging Features to Assess Early Response and Predict Prognosis in Oropharyngeal Cancer. *J Nucl Med* 2020;61:327-36.
  23. Lu J, Liao J, Chen Y, et al. Risk factor analysis and prediction model for papillary thyroid carcinoma with lymph node metastasis. *Front Endocrinol (Lausanne)* 2023;14:1287593.
  24. Zhang H, Ogasawara K. Grad-CAM-Based Explainable Artificial Intelligence Related to Medical Text Processing. *Bioengineering (Basel)* 2023;10:1070.
  25. Jia X, Ma Z, Kong D, et al. Novel Human Artificial Intelligence Hybrid Framework Pinpoints Thyroid Nodule Malignancy and Identifies Overlooked Second-Order Ultrasonographic Features. *Cancers (Basel)* 2022;14:4440.
- (English Language Editor: J. Jones)

**Cite this article as:** Ni Z, Zhou T, Fang H, Lin X, Xing Z, Li X, Xie Y, Hong L, Huang S, Ding J, Huang H. Radiomics and deep learning for large volume lymph node metastasis in papillary thyroid carcinoma. *Gland Surg* 2024;13(9):1639-1649. doi: 10.21037/gs-24-308